ResearchGate

See discussions, stats, and author profiles for this publication at: https://www.researchgate.net/publication/231649700

Elucidation of Charge Transport and Optical Parameters in the Newly 1CR-dppm Organic Crystalline Semiconductors

ARTICLE *in* THE JOURNAL OF PHYSICAL CHEMISTRY C · AUGUST 2008

Impact Factor: 4.77 · DOI: 10.1021/jp801199a

CITATIONS
5

READS
17

3 AUTHORS, INCLUDING:

Ahmed Al hossiny
Assiut University
9 PUBLICATIONS **27** CITATIONS

SEE PROFILE

Available from: Ahmed Al hossiny
Retrieved on: 29 January 2016

THE JOURNAL OF PHYSICAL CHEMISTRY C

Subscriber access provided by KYUSHU UNIV 00A

Article

Elucidation of Charge Transport and Optical Parameters in the Newly 1CR-dppm Organic Crystalline Semiconductors

A. M. Badr, A. A. El-Amin, and A. F. Al-Hossainy

J. Phys. Chem. C, **2008**, 112 (36), 14188-14195 • DOI: 10.1021/jp801199a • Publication Date (Web): 15 August 2008

Downloaded from http://pubs.acs.org on December 26, 2008

More About This Article

Additional resources and features associated with this article are available within the HTML version:

- Supporting Information
- Access to high resolution figures
- Links to articles and content related to this article
- Copyright permission to reproduce figures and/or text from this article

View the Full Text HTML

ACS Publications
High quality. High impact.

The Journal of Physical Chemistry C is published by the American Chemical Society. 1155 Sixteenth Street N.W., Washington, DC 20036

Elucidation of Charge Transport and Optical Parameters in the Newly 1CR-dppm Organic Crystalline Semiconductors

A. M. Badr,*,† A. A. El-Amin,† and A. F. Al-Hossainy‡

Physics Department, Chemistry Department, Faculty of Science, South Valley University, Aswan, Egypt

Received: February 10, 2008; Revised Manuscript Received: June 4, 2008

As a part of a wide plan concerning the novel organic materials, a set of newly organic semiconductors has been obtained in our laboratories. In this paper, a clear overview was reported for elucidating the preparation processes of the chromium−copper mixed crystals. In line with the novel pyrazole diphenylphosphino-methane (M-dppm) derivatives, two mixed organic semiconductors were obtained: the one cupper apyrazole ring compound 5a, $C_{78}H_{74}CrCuN_4O_3P_4$ (1CR-dppm) and the two cupper apyrazole ring compound 6a, $C_{78}H_{74}CrCu_2N_4O_4P_4$ (2CR-dppm). The structure of the obtained crystals were examined by the X−ray diffraction, and the structures of the two mentioned compounds were discussed based on elemental analysis (EA), IR, ^{1}H NMR, ^{31}P NMR spectroscopic data, and fast atom bombardment mass spectra. The compounds under investigation show typical semiconductor behavior due to of delocalization of the π-electrons in the structure. The temperature dependence of charge transports and optical parameters for the 5a crystals ($C_{78}H_{74}CrCuN_4O_3P_4$) were investigated and discussed in this work. This study was carried out with the aids of the transmittance and reflectance spectra in the temperature range 77−300 K. The reflectance and transmittance spectra were measured for the 5a organic crystalline semiconductors over the incident photon energy range 1.3−2.5 eV. These spectra were used for determining the optical parameters and elucidating the charge transport in the 5a compound.

1. Introduction

Low-molecular weight materials and polymers[1] are two major classes of organic semiconductors that have in common a conjugated π-electron system formed by the p_z orbitals of sp^2-hybridized C atoms in the molecules. In comparison to the σ bonds constituting the backbone of the molecules, π-bonding is significantly weaker. Therefore, the lowest electronic excitations of conjugated molecules are the $\pi-\pi^*$ transitions with an energy gap typically between 1.5 and 3 eV leading to light absorption or emission in the visible spectral range. The electronic properties of a molecule depend on factors like the conjugation length and the presence of electron donating or withdrawing groups. Thus, organic chemistry offers a wide range of possibilities to tune the optoelectronic properties of organic semiconducting materials. A number of low-molecular weight materials can be grown as single crystals allowing intrinsic electronic properties to be studied on such model systems. Growth of highly ordered thin films either by vacuum deposition or by solution processing is still a subject of ongoing research but will be crucial for many applications.[2] Despite the fast developments in the field of organic electronics and dramatic improvement in knowledge and manipulation of the charge injection and transport in organic semiconductors, a reliable relationship between microscopic properties and their effect on the physical properties is still under development, whereas several investigations have been done in understanding the mechanism of conduction in organic semiconductors. In order to elucidate fundamental questions regarding charge transport in the above-mentioned materials, correct correlations among the morphology, the molecular packing, and the resulting electronic properties are essential. In organic molecular solids, the intermolecular forces are weak (van der Waals and electrostatic type), where the bonding energies are considerably lower than in covalent and ionic inorganic semiconductors.[3,4] Consequently, the mechanism of charge transport is fundamentally different. In organic semiconductors, the charge carriers interact strongly with the lattice environment leading to polarization effects and tendency of charge carrier localization. The weak van der Waals interactions result in a small electronic bandwidth, strong electron−lattice interaction, and polaron formation.[5–10]

The work goals were planned not only for improving the performance of organic materials for possible incorporation in devices, but also for satisfying the pressing need for insight into the relevant physical processes that govern the charge transport in these materials. This emphasizes the importance of the control of defects and impurity states in organic molecular crystals in order to obtain the desired photoelectrical properties.

2. Experimental Setup and Apparatus

2.1. Synthesis and Structural Properties. In this experiment, liquid ammonia was used to prepare a diphosphine that can potentially serve as a bidentate ligand for transition metals. In the first step of the synthesis, advantages of the strongly reducing nature of sodium-ammonia solutions were employed to add two electrons to triphenylphosphine, which was resulted in cleavage of a carbon−phosphorus bond. As a result of this reaction, a product of phenylsodium is the conjugate base of benzene. Owing to its high basicity, ammonia was deprotonated using NaC_6H_5 quickly to give benzene and $NaNH_2$. By adding NH_4Br, the resulting solution of $NaNH_2$ can be neutralized. Another product of the cleavage of $P(C_6H_5)_3$ with Na/NH_3 solution was found to be sodium diphenylphosphide $NaP(C_6H_5)_2$. Sodium diphenylphosphide $NaP(C_6H_5)_2$ is a yellow

* To whom correspondence should be addressed.
† Physics Department.
‡ Chemistry Department.

10.1021/jp801199a CCC: $40.75 © 2008 American Chemical Society
Published on Web 08/15/2008

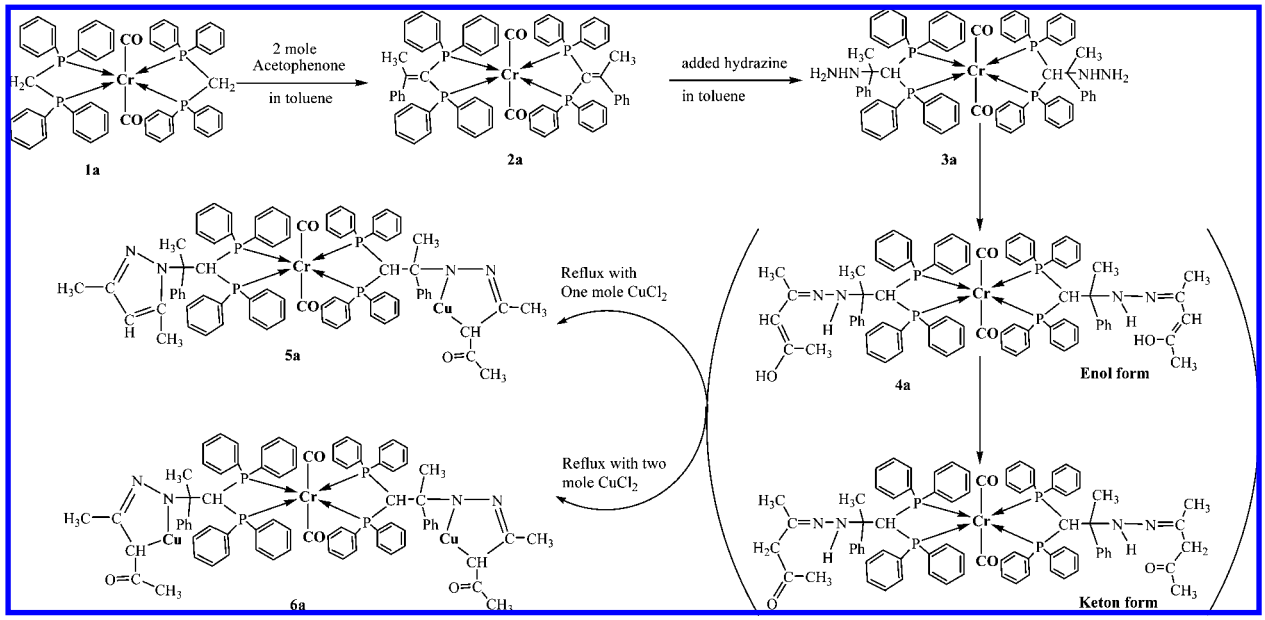

Figure 1. The schematic diagram that describes the formation of the 1CR-dppm crystals.

salt that is soluble in polar solvents such as ammonia. Because it is very easily oxidized, sodium diphenylphosphide $NaP(C_6H_5)_2$ was protected from air.

$$P(C_6H_5)_3 + 2Na \rightarrow NaP(C_6H_5)_2 + NaC_6H_5$$

$$NaC_6H_5 + NH_3 \rightarrow NaNH_2 + C_6H_6$$

$$NaNH_2 + NH_4Br \rightarrow NaBr + 2NH_3$$

Thereafter, the reaction of $NaP(C_6H_5)_2$ with dichloromethane was achieved to give the bis-(diphenylphosphino) methane, $(C_6H_5)_2PCH_2P(C_6H_5)_2$.[11]

$$2NaP(C_6H_5)_2 + ClCH_2Cl \rightarrow (C_6H_5)_2PCH_2P(C_6H_5)_2 + 2NaCl$$

Synthesis and the preparation conditions for the newly $C_{78}H_{74}CrCuN_4O_3P_4$ and $C_{78}H_{74}CrCu_2N_4O_4P_4$ organic crystalline semiconductors were depicted in the schematic reactions shown in Figure 1. The structural data of the obtained organic compounds was estimated and discussed on the basis of elemental analysis (EA), IR, ^{1}H NMR, ^{31}P NMR spectroscopic data, and fast atom bombardment (FAB) mass spectra (see Table 1 and Figure 2).

The complex [2a, $\{(Ph_2P)_2C{=}CCH^1{}_3(Ph)\}Cr(CO)_2\{(Ph_2P)_2C{=}CCH^2{}_3(Ph)\}$] was obtained by the treatment of the chromium-diphosphino adduct in benzene with 20% slight excess of acetophenone. After heating ca. 3 h under dinitrogen, a pale brown crystals of the chromium (diphosphino) acetophonen adduct were found in >70% yield. By the treatment of the chromium-aceophonen adduct in benzene with 20% slight excess of hydrazine hydrate and after heating ca. 1 h under dinitrogen, pale brown crystals of the chromium hydrazine adduct were found in >80% yield, the resultant compound, the complex [3a, $\{(Ph_2P)_2CH^1CNH^2NH^3{}_2CH^4{}_3(Ph)\}Cr(CO)_2\{(Ph_2P)_2CHNNH_2$-$CCH_3(Ph)\}$], was obtained. A suspension solution of the 3a compound was reacted with copper dichloride, and then with acetylacetone to give a copper pyrazole derivaties ring. In addition, on heating the chromium-hydrazines adduct with one equivalent mole and two equivalents of acetylacetone in toluene for a prolonged period ca. 16 h, a pale brown crystalline product was formed (5a). The structure of this complex was formulated based on (i) satisfactory elemental analysis; (ii) the $^{31}P-\{^1H\}$ NMR spectrum that showed a singlet at $\delta = -80$ ppm with ^{52}Cr satellites. The $^1H-\{^{31}P\}$ and ^{1}H NMR spectra showed ten signals (see Figure 2). At $\delta = 6.32$ and $\delta = 6.07$ ppm, a triplet of relative intensity 1H was observed and assigned to CH^1 proton and CH^6. Two singles of relative intensity 1H at $\delta = 5.33$ and $\delta = 4.10$ p.p.m were observed and assigned to ($-N-N{=}C-CH^4$) and ($-N-N{=}C-CH^8$) proton coupling with CH_3 protons, $^4J(CH-C-CH_3^5) = 2.5$ Hz and $^4J(CH-C-CH_3^{10}) = 3.4$ Hz. Four strong singles were observed at $\delta = 2.10$, $\delta = 2.35$, $\delta = 2.55$, and $\delta = 2.94$ ppm of relative intensity 12H and assigned to CH_3^{10}, CH_3^5, CH_3^9, and CH_3^3 protons. Two singlets were observed at $\delta = 2.53$ ppm and $\delta = 2.17$ ppm of relative intensity 3H, each assigned to two methyl protons CH_3^2 and CH_3^7 that are difficult to be distinguished. The ^{1}H NMR spectrum also shows coupling to phosphorus by the CH^1 proton, the signal being a triplet of triplets, $^3J(PCH) = 16$ Hz. The infrared spectrum was obtained for characterizing the cis-chelated tetracarbonyl complex, where the υ(N−H) band at 3320 of the starting material was absent. A suspension solution of chromiumdiphosphinohydrazine[$\{(Ph_2P)_2CHCNHNH_2CH_3(Ph)\}$-$Cr(CO)_2\{(Ph_2P)_2CHNNH_2CCH_3(Ph)\}$] complex was reacted with copper dichloride to give a copper pyrazole derivates ring. Moreover, on heating a mixture of one equivalent of the chromium-hydrazine adduct, two equivalents mole of copper dichloride and one equivalent mole of acetylacetone in toluene for a prolonged period ca. 16 h, a pale brown crystalline product was formed (6a). The structure of this complex was formulated based on (i) satisfactory elemental analysis; (ii) The $^{31}P-\{^1H\}$ NMR spectrum that showed a singlet at $\delta = 55$ ppm with ^{52}Cr satellites, $^1J(CrP)/Hz = 0$ (see Table 1 for data); (iii) the $^1H-\{^{31}P\}$ and ^{1}H NMR spectra, showed five signals. At $\delta = 6.65$ ppm a triplet of relative intensity 2H were observed and assigned to CH^1 proton. A single of relative intensity 2H at $\delta = 5.60$ ppm was observed and assigned to ($-N-N{=}C-CH^3$) proton coupling with CH_3 protons, $^4J(CH-C-CH_3^5)$=2.5 Hz. A strong one was observed at $\delta = 2.54$ ppm of relative intensity 3H and assigned to CH_3^2 protons. Two singlet were observed at $\delta = 2.07$ ppm and $\delta = 1.00$ ppm of relative intensity 3H each and assigned to two methyl protons CH_3^4 and CH_3^5. It is

TABLE 1: Characterization Data of the Newly Synthesized Cr−Cu (Diphenylphosphino)Methane Derivative Complexes

mol formula (mol wt), No.	calcd % (found %) C	H	N	mp °C	infrared[a] (υ Cr−CO)cm^{-1} (υ P−C)/cm^{-1}	coupling constants (Hz) $^2J(PCH_2)$/ Hz	$^4J(PCH_3)$/ Hz	$^2J(PCH)$/Hz	NMR($C_2H_2Cl_4$/ $(CD_3)_2CO$) δ, ppm, Assignment	δ(P)/ppm	*m/z*
$C_{52}H_{46}CrO_2P_4$ (878), 1a	71.07 (7059)	5.28 (5.30)		209−212	2005s, 1980w, 1189w, 186 5sb, 725s, 690s	11			2.43(m,4H, 2 group CH_2 methylene) {6.91(s, 8H, p-CH)}, {7.12(s, 16H, o−CH)} {7.50(s, 16H, m-CH)} aromatic ring	55.43	989.19
$C_{68}H_{58}CrO_2P_4$ (1083.08) 2a	75.41 (75.12)	5.40 (5.45)		217−220	2010s, 1984w, 1195w, 186 5sb, 710s, 690s	−	6	−	1.63s, 6H, 2 group CH_3 methyl) {6.93(s, 8H, p-CH)}, {7.03(s, 16H, o−CH)} {7.55(s, 16H, m-CH)} aromatic ring 2.45(wb, 1NH, $2NH_2$, amine)	50.11	1082.28
$C_{68}H_{66}CrN_4O_2P_2$[c] (1146.35)3a	71.20 (71.34)	5.80 (5.83)	4.88 (4.84)	196−200	200s, 1981w, 1892w, 186 0b, 715s, 680s		6	14	5.72(w, 1H, methine, 1 beta−N) 1.76(s, 3H, methyl-CH)) {6.85−7.57(s, 8H, 16H, 16H)} aromatic ring 6.32(w, 1H,methine, 1beta-N) 6.07(w, 1H,methine, 1beta-N) 5.33(s, 1H, 1−pyrazole, 1alpha−N−N=C−C1) 4.10(s, 1H, 1−pyrazole, 1alpha−N−N=c−C1)	48.90	1147.35
$C_{78}H_{74}CrCuN_4O_3P_4$ (1354.88) 5a	69.14 (69.43)	5.51 (5.37)	4.03 (3.96)	189−200	200s, 1980w, 1890w, 186 5sb, 710s, 685s		10 8	15 12	2.53(s, 3H, methyl, 1beta-N) 2.17(s, 3H, methyl, 1beat-N) 2.23(s, 3H, methyl, 1 alpha−N−N=C−1) 2.10(s, 3H, methyl, 1 alpha−N−N=C−1) 2.36(s, 3H, methyl, 1 alpha−N−N=C−CH=C−1) 2.55(s, 3H, methyl, 1 alpha−N−N=C−CH=C−1) {6.83−7.55(m, 8H, 16H, 16H)} aromatic ring 6.65(w, 1H,methine, 1beta-N) 5.60(s, 1H, 1−pyrazole, 1alpha−N−N=C−C1) 2.54(s, 3H, methyl, 1beta-N)	50.50	1432.27
$C_{78}H_{74}CrCu_2N_4O_4P_4$ (1434.43) 6a	65.31 (65.28)	5.20 (5.11)	3.91 (3.95)	230−237	2005s, 1980w, 1890w, 186 0b, 720s, 680s				1.00(s, 3H, Methyl, 1 alpha−N−N=C−1) 2.07(s, 3H, methyl, 1 alpha−N−N=C−CH=C−1) {6.80−7.55(m, 8H, 16H, 16H)} aromatic ring		

[a] Infrared spectra in KBr discs: Strong (s), Weak (w), (m) Medium, (wb) Weak Board and (b) Board. [b] Chemical shifts, δ, to high frequency of 85% H_3PO_4 [c] υ(NH) = 3300 cm^{-1}.

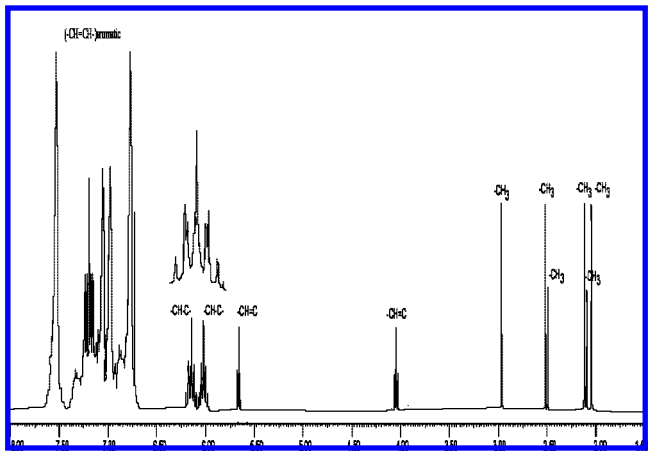

Figure 2. Shows the $^1H-\{^{31}P\}$ and ^1H NMR spectra for the 1CR-dppm crystals.

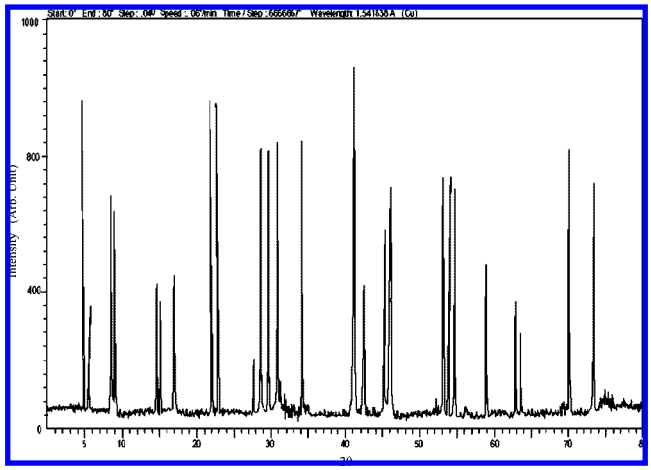

Figure 3. Shows the X-ray diffraction pattern of the 1CR-dppm crystals.

difficult to distinguish between the two as indicated by the ^1H NMR spectrum. That shows coupling to phosphorus by the CH^1 proton with the signal being a triplet of triplets, $^3J(PCH) = 20$ Hz.

2.2. Preparing the Samples and Apparatus. The melting points were recorded on a Galenkanp melting point apparatus. Elemental analyses were carried out at the Micro Analytical center (Assiut University). The IR spectra (KBr) were determined on a Shimadzu corporation Chart 200−91527 spectrophotometer. ^1H NMR spectra were recorded with a Bruker AMX-250 spectrometer. Mass spectra were recorded on HpMs 6988 spectrometer and electron-impact (EI). The X-ray data were collected with a radiation of $\lambda = 1.541838$ Å for the crystalline natures of the solidified materials (see Figure 3). The bulk sample, which was used in the optical measurements, was prepared by splitting the crystal along the cleavage plane and hence the resultant surface was mirrorlike without any mechanical treatment. Then the obtained samples were treated to be in a circular shape of thickness ~0.25 cm. The treated samples were mounted individually on the coldfinger inside optical cryostat (Oxford DN1704-type), which was evacuated to about 10^{-5} Torr. With the aids of a piece of aluminum foil that was mounted on the finger of the holder, a hole was established in the foil to be perpendicular to the monochromatic beam; the hole surface was smaller than the sample surface. A digital temperature controller (Oxford ITC601-type) controlled the temperature inside the cryostat. A UV−vis double beam spectrophotometer of model UV-1650PC was employed for recording the reflectance, transmittance, and absorbance spectra. These spectra were measured over the incident photon energy of the wavelength range from 494 to 951 nm in the temperature range 77−300 K. In this work, the temperature dependence of charge transports and optical parameters were investigated and discussed for the newly organic crystalline semiconductors 5a ($C_{78}H_{74}CrCuN_4O_3P_4$).

TABLE 2: UV/vis Data for Phosphino-substituted Hydrazine Chromium Complexes in CH_2Cl_2

compound	λ_{max}/nm (ε/L mol^{-1} cm^{-1})	λ_{max}/nm (ε/L mol^{-1} cm^{-1})
$C_{52}H_{46}CrO_2P_4$ (1a)	468 (634)	618 (430)
$C_{68}H_{58}CrO_2P_4$ (2a)	454 (743)	609 (590)
$C_{68}H_{66}CrN_4O_2P_4$ (3a)	435 (670)	592 (630)
$C_{78}H_{74}CrCuN_4O_3P_4$ (5a)	421 (962)	573 (530)
$C_{78}H_{74}CrCu_2N_4O_4P_4$ (6a)	412 (735)	569 (641)

3. Results and Discussion

3.1. Electronic Transitions in the Newly 1CR-dppm Organic Semiconductor. In the connection with the orbitals involved in the electronic transition, the difference in energy between the lowest unoccupied molecular orbital (LUMO) and the highest occupied molecular orbital (HOMO) is considerably greater than the activation energy (A) for the transition from the singlet ground-state S_0 to the singlet excited-state S_1. The difference rises from the different electronic interactions (Coulomb term J, exchange term of 2K). The singlet−triplet splitting in this approximation is 2K, where $K > 0$ for the lowest triplet state T_1 and is always below S_1. Due to the configurational interaction, the HOMO−LUMO transition is not necessarily the lowest transition $S_0 \Rightarrow S_1$.[12] The long wavelength absorption energy corresponds to the energy of the HOMO−LUMO gap.[13–15] However, solvent effects and transitions involving the SHOMO and SLUMO (and potentially other MOs), as well as changes in relative orbital energies and electron configurations, can significantly complicate the situation to the extent that one can generally only get meaningful information by comparing closely related compounds.[16] A classification of the electronic transitions (bands) can be made from knowledge of the molecular orbitals (MOs) involved. From occupied bonding σ- or π-orbitals or from nonbonding n-orbitals (lone pair's electrons), an electron can be raised to an empty antibonding σ^{*-} or π^{*-} orbitals. Correspondingly, the electronic transitions (bands) are indicated as $C \Rightarrow \sigma^*$, $\pi \Rightarrow \pi^*$, $n \Rightarrow \sigma$, and $n \Rightarrow \pi$. If the absorbance is determined for all λ or υ and from that the substance-specific value ε, the absorption plot $\varepsilon(\upsilon)$ or $\varepsilon(\lambda)$ can be obtained and thus the UV or UV/vis spectrum. The width (in energy terms) of the electronic states can be described via the band spectrum. The individual bands were characterized by their properties of position, intensity, shape, and fine structure.

The electronic absorption spectral data λ_{max} and ε_{max} values for the synthesized diphosphine derivatives chromium complexes (1a, 2a, 3a, 5a, and 6a) in dichloromethane were viewed in Table 2. The visible absorption spectra of these chromium complexes exhibit various absorption bands within the wavelength range 350−700 nm (see Figure 4). These absorption bands depend primarily on the terminal group (hydrazine derivatives), their linkage position,[17,18] and the type of the transient metal complex. The visible absorption maxima of diphosphine derivatives chromium (dppm) complexes in CH_2Cl_2 undergo bathochromic or hypsochromic shifts depending on the nature of the alphatic and aromatic aldehydes and ketones

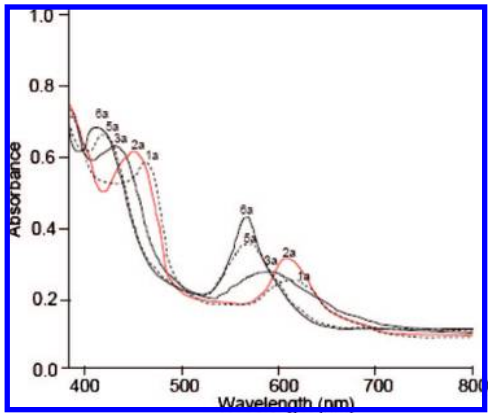

Figure 4. Typical UV/vis spectra of phosphino-substituted transition (Cr−Cu) complexes in CH_2Cl_2.

(undergo condensations reaction) give complex 2a. Thus, substituting A = methylene group in compound 1a typically would exhibit two UV/vis absorption bands (with extinction coefficients of between 634 and 430 L mol^{-1} cm^{-1}), one near 468 nm and the other near 618 nm. These bands are likely to be d−d transitions since the HOMO is largely metal based and the extinction coefficients are less than 1000 L mol^{-1} cm^{-1}. For compound 2a, it was found that there are two UV/vis absorption bands (ε = between 743 and 590 L mol^{-1} cm^{-1}), one near 454 nm and the other near 609 nm. These bands are likely to be d−d transitions since the HOMO is largely metal based and the extinction coefficients are less than 1 000 L mol^{-1} cm^{-1}. Moreover, observe that the two bands of UV/vis spectra that compound 2a changed from (first band, 468−454, and another, 618−609 nm) is shifted to less wavelength (a bathochromic shift). UV/vis absorption bands changed from 1a to 3a (first band, 468−435; the other, 618−592 nm). The shift of bands to lower wavelength between the first band at 33 nm and another at 26 nm) should be a bathochromic shift, whereas for 1a−3a, all of the second UV/vis absorption peaks are broadband; this mean that there complexes that do not contain conjugated double bonds (expected phenyl group). In respect of the two pyrazole derivatives ring 5a, it was found that there are two UV/vis absorption bands (ε = between 962 and 530 L mol^{-1} cm^{-1}), one near 421 nm and the other near 573 nm. The extinction coefficients are less than 1000 L mol^{-1} cm^{-1}. In addition, it was observed that the two band of UV/vis spectra for the compound 5a changed from the first band of 468−421 and another band of 618−573 nm to lower wavelength is a bathochromic shift, whereas, the shift of bands to lower wavelength is between 47−45 nm. For the Cr−Cu pyrazole derivatives ring (6a), two UV/vis absorption bands were found (ε = between 962 and 530 L mol^{-1}cm^{-1}), one near 412 nm and the other near 569 nm. The extinction coefficients are less than 1000 L mol^{-1} cm^{-1}. Moreover, it was observed that the two bands of UV/vis spectra for the compound 6a that changed from the first band of 468−412 nm and another band of 618−569 nm shifted to lower wavelength is a bathochromic shift. Whereas, the shift of bands to lower wavelength is between 56−49 nm.

The UV/vis absorption bands are noted to have been changed from 5a and 6a and all of the second UV/vis absorption peaks are sharp bands, which means that the complexes contained conjugated double bonds in pyrazole derivates ring and phenyl group. Apparently, the σ* orbitals of the dicarbonyl chromium metals groups have a significant influence on the pyrazole ring MOs that affect the bands in the UV/vis spectra. It is obvious

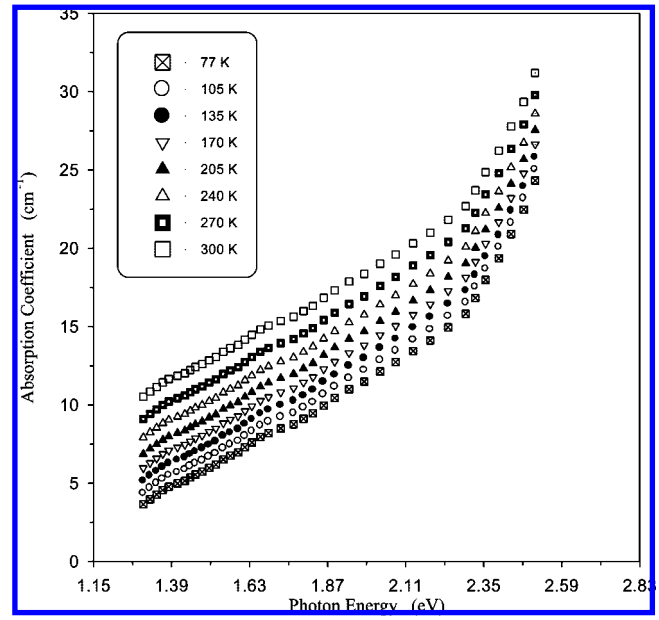

Figure 5. The photon energy dependence of absorption coefficient in the 1CR-dppm crystals.

from Figure 4 that the pyrazole derivatives ring 5a and Cr−Cu pyrazole derivatives ring 6a both exhibit two bands in the UV/vis spectra and that these occur at similar energies. Although there is no extinction, coefficients for the high-energy band are over 1000 L mol^{-1} cm^{-1}. So in accordance with the UV/vis spectra for both derivatives 1a−6a, it was observed that a ligand is assigned to metal in the charge transfer (LMCT) process from diphenylphosphino to a d^0 metal center in the complexes rather than a d−d transition of the copper atom. One must be careful, therefore, when making comparisons between these derivates. These bands are likely to be d−d transitions, whereas the HOMO is largely metal based[19,20] and the extinction coefficients are less than 1000 L mol^{-1} cm^{-1}.

3.2. Photoelectrical Transports and Optical Parameters. Transmittance and reflectance spectra were investigated for the newly 1CR-dppm organic crystalline semiconductors in the temperature range 77 to 300 K. The above-mentioned spectra were measured over the incident photon energy range 1.3 to 2.5 eV. In accordance with the obtained plots, typical spectra were observed in the whole investigated range of temperature. As it is known, optical measurements are productive tools for understanding the band structure, energy gap width and optical parameters of both crystalline and amorphous nonmetallic materials. The optical absorption coefficient (α) is related to the transmittance (T) of a sample with thickness (d) through the relation

$$\alpha = \frac{1}{d}\ln\left(\frac{1}{T}\right) \quad (1)$$

Using this relation, the α − E was described for the 1CR-dppm crystals (see Figure 5). The values of the absorption coefficient were calculated for all investigated temperatures and over the whole investigated range of the incident photon energy. Figure 5 was plotted for all investigated temperatures in the photon energy range 1.3−2.5 eV. This figure also did not show any tails in the low energy region, which indicates that the obtained crystals were grown with high purity, whereas in the low energy region it may be observed that the absorption coefficient exhibits a long band tail at low energies that has most likely originated from defects and impurity states within

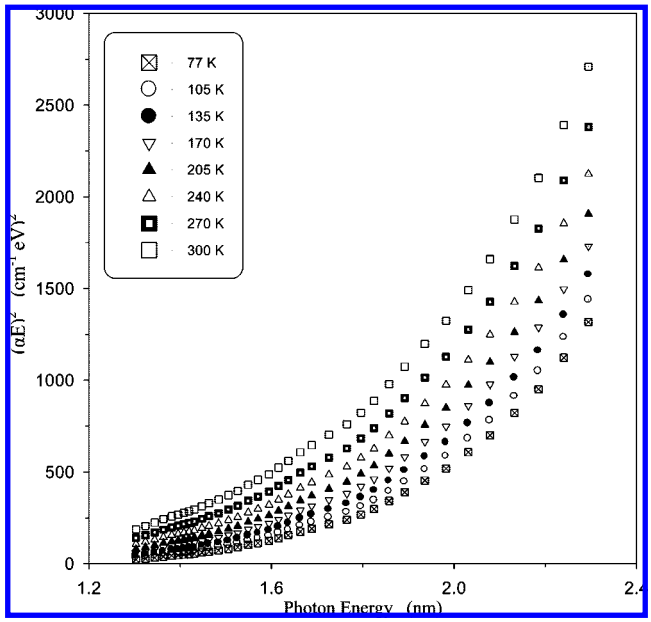

Figure 6. The graph shows the quantity $(\alpha h\upsilon)^2$ as a function of $(h\upsilon)$ for the 1CR-dppm crystals.

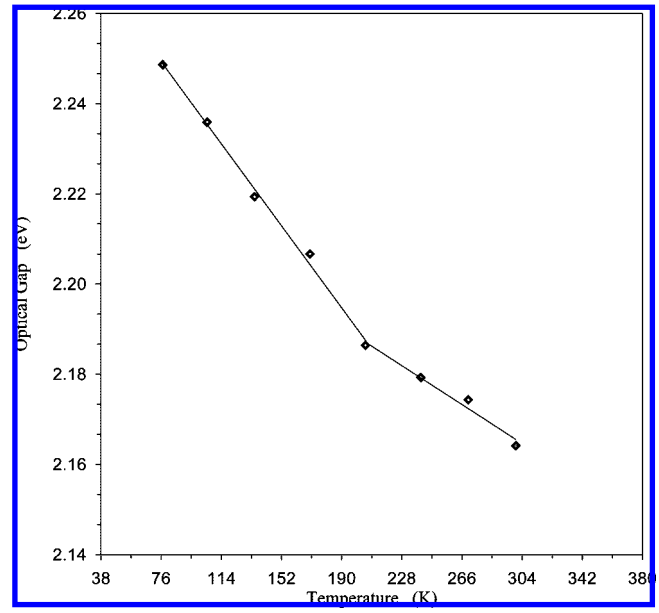

Figure 7. The graph shows temperature dependence of the direct band gap in the 1CR-dppm crystals.

the band gap. Tailing of the band states into the gap width may be induced from a large concentration of free carriers resulting from screened Coulomb interaction between carriers that perturbs the band edges. In the low photon energy region and near the fundamental edge, the absorption coefficient steeply increases with the increase in the photon energy. In the region of the photon energy with the values greater than that of the exponential edge region, the absorption coefficient linearly increases with increasing the incident photon energy (high absorption region).

The relation[21,22] governs the relationship between the absorption coefficient and the incident photon energy ($h\upsilon$) in the high absorption regions (linear increase of α with increase in incident photon energy)

$$\alpha = \frac{1}{h\upsilon}[A(h\upsilon - E_g)^n] \quad (2)$$

where A is constant that depends on the transition probability, E_g is the width of the band gap, and n is an index that characterizes the optical absorption processes in the 1CR-dppm crystals. Analysis of experimental results showed that a proportionality is revealed between the absorption coefficient and the frequency of the photon energy in the form $(h\upsilon - E_g)^n$. The exponent n should be one of the four values 2, 1/2, 3, and 3/2, where the type of the optical transition can be defined in the 1CR-dppm crystals via the above-mentioned values. Theoretically, n is equal to 2, 1/2, 3, or 3/2 for the indirect allowed, direct allowed, indirect forbidden, and direct forbidden transitions respectively.[23] On other hand, the usual method for determining the type of the optical transition includes plots of $(\alpha h\upsilon)^{1/n}$ versus the incident photon energy ($h\upsilon$). These proportionality gives a set of plots with four values of the exponent n: $(\alpha h\upsilon)^{1/2} - h\upsilon$, $(\alpha h\upsilon)^2 - h\upsilon$, $(\alpha h\upsilon)^{1/3} - h\upsilon$, and $(\alpha h\upsilon)^{2/3} - h\upsilon$. One of these plots satisfies the widest linearity of data, and hence its exponent determines the type of the optical transition. In the case of the 1CR-dppm crystals, the exponent n indicates that the dominant transition is a direct allowed one. Therefore, $(\alpha h\upsilon)^2$ was plotted against $(h\upsilon)$ and this graph is described in Figure 6 (also this figure was plotted for all investigated temperatures in the photon energy range 1.3−2.5 eV). In this work, the optical band gaps were calculated by linearly fitting the high absorption regions. These fittings intersect the $h\upsilon$-axis at the values of the optical band gap widths of the 1CR-dppm crystals at the values of temperature under investigation. The estimated values of the gap widths were plotted against the investigated temperatures (see Figure 7) for studying the temperature coefficient (dE_g/dT) of the optical gap in the 1CR-dppm crystals. This figure suggests that the 1CR-dppm organic semiconductor has two temperature coefficients of the optical gap where two linear portions were observed in the mentioned figure: one at the temperature range 77−205 K and the second at the temperature range 205−300 K. These coefficients ascertain that there is an electron−lattice interaction, which depends strongly on temperature; at temperatures much lower than the Debye temperature,[21] where as the temperature increases, the lattice expands and the oscillations of the atoms around their equilibrium lattice points increase. The gap width varies proportionality to the square of the temperature, whereas much above the Debye temperature the gap width varies linearly with the temperature. The following empirical relation has fit the temperature dependence of the band gap with for many semiconductors

$$E_g(T) = E_g(0) - \left(\frac{\alpha T^2}{T+\beta}\right) \quad (3)$$

where, $E_g(0)$ is the value of the energy gap at 0° K, and α and β are constants. With the aids of the mentioned relation and Figure 7, both of α and β were estimated in the temperature range of 77−300 K to be $\sim 4 \times 10^{-4}$ and 48.76, respectively. The temperature coefficients of the optical gap width were calculated for the 1CR-dppm organic semiconductor to be: $\sim -4.79 \times 10^{-4}$ eV in the temperature region 77−205 K and $\sim -2.27 \times 10^{-4}$ eV in the temperature region 205−300 K.

For the transparent range, the reflectance spectra can used for determining the refractive index n of the 1CR-dppm crystals in the whole investigated range of temperature with the aids of the following relation

$$R = [(n-1)/(n+1)]^2 \quad (4)$$

The calculated values of the refractive index were employed for plotting the $n - E$ relation of the above-mentioned organic

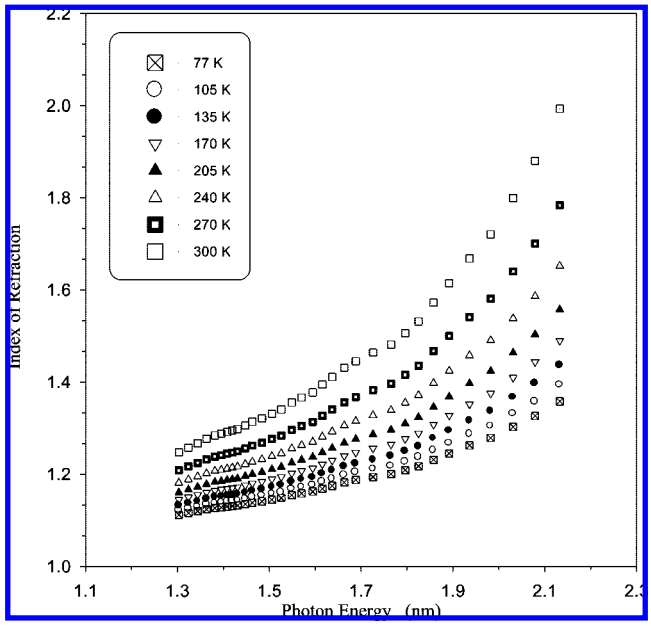

Figure 8. The graph shows dependence of refractive index (n) on the incident photon energy.

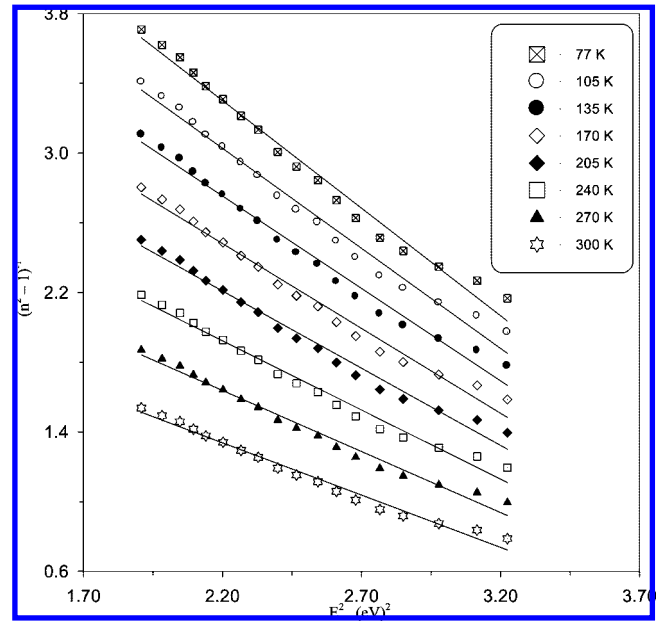

Figure 9. The graph shows quantity $(n^2 - 1)^{-1}$ as a function of $(h\upsilon)^2$ for the 1CR-dppm crystals.

semiconductors for the whole investigated temperatures over the whole investigated range of the incident photon energy (see Figure 8). It is clear from this figure that in the long wavelength region of the investigated photon energy range, the dispersion of the refractive index is normal for the whole investigated temperatures under investigation and can well be described using a single oscillator model[24]

$$n^2 = 1 + \frac{E_o E_d}{E_o^2 - (h\upsilon)^2} \Rightarrow (n^2 - 1)^{-1} = \frac{E_o}{E_d} - \left(\frac{1}{E_o E_d}\right)(h\upsilon)^2 \quad (5)$$

where, E_o is the single oscillator energy, E_d is the dispersion energy, and $(h\upsilon)$ is the incident photon energy.

It is evident from Figure 8 that the refractive index of the 1CR-dppm crystals linearly increases with the increase in the incident photon energy in the low energy region 1.38−1.79 eV for the completely investigated temperatures. In addition, there is a considerable change in the refractive index through the variation of temperature. Both the single oscillator energy (E_o) and the dispersion energy (E_d) can be obtained for the investigated temperatures by plotting $(n^2 - 1)^{-1}$ as functions of the photon energy ($h\upsilon$) in the long wavelength region of the investigated range of the photon energy (from 1.38 to 1.79 eV). The above-mentioned relation is depicted in Figure 9. With the aids of this figure, the E_d and E_o were calculated from the slope $(E_o E_d)^{-1}$ and the intercept (E_o/E_d). The calculated values of oscillator energies (E_o), dispersion energies (E_d), and optical band widths (E_g) for the 1CR-dppm organic crystalline semiconductor in the temperature range 77−300 K are summarized in Table 3. The static refractive index $(n(0) = (1 + E_d/E_o)^{1/2})$ and the static dielectric constant $(\varepsilon_s = n^2(0))$ were calculated using the above-reported relation and found to be 1.173 and 1.376, respectively. Data recorded in Table 3 suggests that both the calculated values of the optical gap width and the oscillation energy of the 1CR-dppm crystals decrease with the increase in temperature, but there is a decrease in the dispersion energy with increasing temperature.

TABLE 3: Photoelectrical Transport and Optical Parameters of the 1CR-dppm Crystals

temperature (K)	optical gap (eV)	oscillation energy (eV)	dispersion energy (eV)
77	2.249	2.207	0.367
105	2.236	2.199	0.396
135	2.219	2.189	0.430
170	2.207	2.179	0.471
205	2.186	2.166	0.521
240	2.179	2.149	0.586
270	2.174	2.130	0.670
300	2.164	2.104	0.792

4. Conclusion

The transmittance and reflectance spectra were employed to investigate the photoelectrical transports and optical parameters of the 1CR-dppm organic crystalline semiconductors. The optical measurements were carried out in the incident photon energy range 1.3−2.5 eV over the temperature range 77−300 K. In line with of the $\alpha - E$ relation, it was observed that in the high absorption region, the coefficient of absorbance linearly increases for the 1CR-dppm crystals with the increase in the incident photon energy. The above-mentioned measurements exhibit direct allowed transitions in the investigated organic crystalline semiconductor. With the aids of these measurements, the direct allowed gaps of the 1CR-dppm crystals were calculated for the whole investigated temperatures to be ∼2.164 eV at room temperature. As a result of the optical gap−temperature relation, it was found that the 1CR-dppm organic semiconductor has two temperature coefficients of the optical gap: $\sim -4.79 \times 10^{-4}$ eV at the temperature range 77−205 K and $\sim -2.27 \times 10^{-4}$ eV at the temperature range 205−300 K. In accordance with the linear proportionality of the refractive index for the two investigated semiconductors to the long wavelength region of the incident photon energy, the oscillator E_o, dispersion E_d energies of the refractive index, static refractive index, and static dielectric constant were evaluated for the whole investigated temperatures. Consequently, it was observed that with the increase in temperature, there is overall decrease and increase in the oscillation and dispersion energies, respectively.

Acknowledgment. The author is much indebted to Professor Dr. A. E. Belal (Physics Department, Aswan Faculty of Science, South Valley University, Egypt) for his help and encouragement.

References and Notes

(1) *Organic Electronic Materials*; Farchioni, R.; Grosso, G., Eds.; Springer: Berlin, 2001.
(2) Faupel, R.; Dimitrakopoulos, C.; Kahn, A.; Wöll, C. *J. Mater. Res.* **2004**, *19*, 7.
(3) Pope, M.; Swenberg, C. E. *Electronic Processes in Organic Crystals and Polymers*, 2nd ed.; Oxford University Press: New York, 1999.
(4) Sze, S. M. *Physics of Semiconductor Devices*; Wiley: New York, 1981.
(5) Haddon, R. C.; Chi, X.; Itkis, M. E; Anthony, J. E.; Eaton, D. L.; Siegrist, T.; Mattheus, C. C.; Palstra, T. T. M. *J. Phys. Chem. B* **2002**, *106*, 8288.
(6) Silbey, R.; Jortner, J.; Rice, S. A.; Vala, M. T., Jr. *J. Chem. Phys.* **1965**, *42*, 733.
(7) Brocks, G.; van den Brink, J.; Morpurgo, A. F. *Phys. Rev. Lett.* **2004**, *93*, 146405.
(8) Troisi, A.; Orlandi, G. *Phys. Rev. Lett.* **2006**, *96*, 086601.
(9) Cheng, Y. C.; Silbey, R. J.; da Silva Filho, D. A.; Calbert, J. P.; Cornil, J.; Brédas, J.-L. *J. Chem. Phys.* **2003**, *118*, 3764.
(10) Hannewald, K.; Stojanovic, V. M.; Schellekens, J. M. T.; Bobbert, P. A.; Kresse, G.; Hafner, J. *Phys. Rev. B* **2004**, *69*, 075211.
(11) Gregory, S. G.; Thomas, B. R.; Robert, j. A. *Synthesis and technique Inorganic Chemistry*, 3th ed.; Springer-Verlag: New York, 1999; Part II, pp 85−92.
(12) Enders, D.; Noyori, R.; Trost, B. M. *Spectroscopic methods in organic chemistry*; Thieme, G, Ed.; Verlag Stuttgart: New York, 1997.
(13) Santi, S.; Ceccon, A.; Crociani, L.; Gambaro, A.; Ganis, P.; Tiso, M.; Venzo, A.; Bacchi, A. *Organometallics* **2002**, *21*, 565.
(14) Atwood, C. G.; Geiger, W. E. *J. Am. Chem. Soc.* **2000**, *122*, 5477.
(15) Ward, M. D. *Chem. Soc. Rev.* **1995**, *24*, 121.
(16) Loukova, G. V.; Strelets, V. V. *Collect. Czech. Chem. Commun.* **2001**, *66*, 185.
(17) Abd El−Aal, R. M.; Belal, A. A. M. *Dyes Pigm.* **2005**, *65*, 129.
(18) Rajagopal, R.; Shenoy, V. U.; Padmanabhan, S.; Sequeira, S.; Seshadri, S. *Dyes Pigm.* **1990**, *13*, 167.
(19) O'Hare, D.; Green, J. C.; Marder, T.; Collins, S.; Stringer, G.; Kakkar, A. K.; Kaltsoyannis, N.; Kuhn, A.; Lewis, R.; Mehnert, C.; Scott, P.; Kurmoo, M.; Pugh, S. *Organometallics* **1992**, *11*, 48.
(20) Calhorda, M. J.; Veiros, L. F. *J. Organomet. Chem.* **2001**, *635*, 197.
(21) Pankove, J. I. *Optical processes in Semiconductors*; Dover Publications: New York, 1971; p 93.
(22) Tauc, J. *Amorphous and Liquid Semiconductors*; Plenum: New York, 1974; Chapter 4.
(23) Qasrawi, A. F. *Cryst. Res. Technol.* **2005**, *40*, 610614].
(24) Baban, C.; Rusu, G. I.; Prepelita, P. *J. Optoelectron. Adv. Mater.* **2005**, 817–821.

JP801199A